Concurrence of monoenergetic electron beams and bright X-rays from an evolving laser-plasma bubble

W. C. Yan[1], L. M. Chen[1*], D. Z. Li[2], N. Hafz[3], J. Dunn[4], L. Zhang[1,5], Y. Ma[1], K. Huang[1], L. N. Su[1], M. Chen[3], Z. M. Sheng[3], J. Zhang[3*]

[1]*Beijing National Laboratory of Condensed Matter Physics, Institute of Physics, CAS, Beijing 100080, China*
[2]*Institute of High Energy Physics, CAS, Beijing 100049, China*
[3]*Key Laboratory for Laser Plasmas and Department of Physics and Astronomy, Shanghai Jiao Tong University, Shanghai 200240, China*
[4]*Lawrence Livermore National Laboratory, California 94550, USA*
[5]*Beijing Institute of Control Engineering, Beijing, 100190, China*

Desktop laser-plasma acceleration has proven to be able to generate GeV-level quasi-monoenergetic electron beams[1,2]. Moreover, such electron beams can oscillate transversely (wiggling motion) in the laser-produced plasma bubble/channel and emit collimated ultrashort X-ray flash known as betatron radiation with photon energy ranging from keV to MeV[3]. This implies that usually one cannot obtain both bright betatron X-rays and high quality electron beams with low emittance simultaneously in the same accelerating wave bucket. Here, we report the first experimental observation of two distinct electron bunches in a single laser shot, one featured with quasi-monoenergetic spectrum and another with continuous spectrum along with large emittance. The latter is able to generate high flux betatron X-rays. Such observation is found only when the laser self-guiding is extended over 4mm. Numerical simulation reveals that two bunches of electrons are injected at different stages due to the bubble evolution. The first bunch is injected at the beginning to form a stable quasi-monoenergetic electron beam, while the second one is injected later due to the oscillation of the bubble size as a result of the change of the laser spot size during the propagation. Due to the inherent temporal synchronization, this unique electron-photon source can be ideal for pump-probe applications with femtosecond time resolution.

* E-mail: lmchen@iphy.ac.cn; jzhang1@sjtu.edu.cn

Synchrotron light sources are powerful in generating bright X-rays for a wide range of applications in basic science, medicine, and industry[4]. However, these machines are usually large in size and expensive for construction and maintenance and are thus unaffordable to broad users. With the advent of table-top ultra-short and ultra-intense lasers, laser-plasma acceleration (LPA) proposed by Tajima and Dawson[5] has demonstrated its great potential as a compact accelerator and X-ray source. Significant progress in LPA was made in the last decade: well-collimated (~mrad) quasi-monoenergetic electron beams were first observed in 2004[6-8], and the electron energy above GeV over cm-scale acceleration length[1,2,9,10] were demonstrated in several laboratories in the last few years.

While accelerating longitudinally in the laser wakefield, the electron beams also oscillate transversally (wiggling motion) due to the transverse structure of the wakefield, which emits well-collimated betatron X-rays[11]. Among several mechanisms to generate X-ray radiation from laser-plasma interactions[12-17], the betatron radiation is straightforward and able to deliver larger X-ray photon flux per shot (10^8 phs/shot[18]) and higher photon energy (up to gamma rays[3]). The betatron oscillation frequency is given by $\omega_\beta=\omega_p(2\gamma)^{-1/2}$, where ω_p is the plasma frequency and γ is the Lorentz factor of the accelerated electron beams. For large-amplitude betatron oscillations (i.e., a few micrometers in size), the resulting broadband spectrum extends up to the critical frequency at $\omega_c\approx2\gamma^2\omega_\beta$, after which it drops exponentially. The radiation is emitted in the forward direction within a cone angle $\theta\approx K/\gamma$, where K is the strength parameter of the plasma wiggler given by $K=2\pi(\gamma r_0)/\lambda_b=1.33\times10^{-10}\gamma^{1/2}n_e^{1/2}[\mathrm{cm}^{-3}]r_0[\mu\mathrm{m}]$. The average photon number with mean energy $\hbar\omega_c$ emitted by an electron is given by $N_x=5.6\times10^{-3}N_\beta K$, where N_β is the number of oscillation periods. Many experiments[2,3,18-21] have been carried out to enhance the radiation flux, for example, to increase the electron charge, the electron energy, the oscillation amplitude r_0, and oscillation period N_β through extending the acceleration length. However, many experiments have shown that the improvement of the betatron X-ray flux always needs to sacrifice the electron beam quality. For example, as mentioned above, since $N_x\propto r_0$, the increasing of r_0 is considered as an efficient way to enhance the x-ray flux, which result in a larger electron emittance and

energy spread.

In this paper, we demonstrate the simultaneous generation of quasi-monoenergetic electron beams and collimated high flux X-ray sources from multiple-injections in self-injected LWFA on a hundred-terawatt (TW) laser system using 1cm long Helium gas jet. Two sequentially injected bunches of electrons are observed in experiment, where the first bunch forms a quasi-monoenergetic spectrum around 0.46 GeV with < 9% energy spread and the second bunch contains more electrons but forms a broad spectrum with highest energy up to 1.4 GeV. Such energy is beyond the energy gain estimated by the usual dephasing-limit[12]. A betatron X-ray flash, which had $4.5\text{x}10^8$ photons per shot and with critical photon energy ~15 keV, was generated simultaneously at a fixed plasma density ($4\text{x}10^{18}$ cm^{-3}). This is higher than the density matched to the blow-out regime[22]. Two-dimensional particle-in-cell (2D PIC) simulations illustrate that the experimental observation can be attributed to sequential injections of two electron bunches as the plasma channel length increases. The first injection is found at early time, which finally forms a stable quasi-monoenergetic electron beam. The second injection appears later as a result of the laser spot size oscillation, leading to the rapid changes of the accelerating bubble structure. The latter is consistent with experimental observation of the bright betatron X-ray flux.

The experimental setup is shown in **Fig. 1**. The laser pulses from the hundred-TW laser system are focused on a helium gas jet nozzle (see Methods for details) to create a fully ionized plasma and to excite a relativistic wakefield (plasma wave) which self-trap and accelerate electrons. Knowing that the critical laser power for relativistic self-guiding in the plasma is given by $P_{cr}(\text{GW})=17.7\omega^2/\omega_p^2$, and the used plasma density of $4\times10^{18}\text{cm}^{-3}$, thus our laser pulses are well above the self-guiding threshold (P =100 TW =13 P_{cr}) and can be self-guided over a long distance (> 1 cm ≅ $10z_R$)[23]. The dephasing length for the accelerated electrons $L_d \sim \lambda_p^3/\lambda_0^2$ is 7 mm at the above density for 800 nm laser wavelength.

Fig. 2a shows a well-collimated (~ 4 mrad) quasi-monoenergetic electron bunch at 180 MeV ($\Delta E/E$~ 10%) that contains 5 pC of charge; the electron bunch is observed for ~ 2 mm channel length, as shown in **Fig. 2f**. Betatron radiation was not observed in this

case. As we increased the incident laser power, the observed channel length was increased to ~ 4 mm (**Fig. 2g**). In the meanwhile, the energy of the qusi-monoenergetic electron bunch approaches 290 MeV ($\Delta E/E$~20%) and a low energy second bunch starts to appear in the spectrum (**Fig. 2b)**. In this laser shot, a weak betatron radiation signal of 2.7×10^7 photons (E_c~15 keV) also appears. For a longer channel of 6 mm realized by further increasing the laser power (**Fig. 2h**), the maximum energy of the second electron bunch surpasses the first bunch. From the **Figs. 2c** and **2k**, the two electron bunches overlap in the energy spectra but are still distinguishable, with central energy ~0.43 GeV for first electron bunch and the maximum energy up to 0.6 GeV for the second one. Correspondingly, the betatron radiation becomes much brighter; 1.2×10^8 photons are detected in this shot. As the laser-plasma channel length reaches to 9 and 10 mm as shown in **Figs. 2i** and **2j,** the electron bunches accelerated beyond 1 GeV contain 60 pC and 90 pC of charge, respectively, as shown in **Figs. 2d** and **2e**. The inset **1** of **Fig. 2k** shows the cut-off (maximum) energy are up to 1.2 and 1.4 GeV with uncertainty of 0.1 GeV at 9 and 10mm channel lengths, respectively. The energy spectra of these two bunches are obviously broad, however, with peaks around 0.5 GeV and 0.35 GeV respectively. The inset **2** of **Fig. 2k** is a typical X-ray beam image with different filters. Considering the attenuating filters between the gas jet and the X-ray detector, the critical energy of the observed betatron radiation (at Image Plate 3) was around 15 keV (see Methods). Moreover, the betatron-radiation increases its brightness with the channel length, which is measured with flux of 2.7×10^8 and 4.5×10^8 photons and divergence angles of ~ 5 and 7 mrad, respectively, for the channel lengths of 9 and 10 mm. These yields of hard X-ray photons amount to ~10-*fold enhancement* compared with those reported earlier[18].

To further understand our experimental results, 2D-PIC simulations have been carried out (see Methods) using similar laser and target parameters. Different normalized laser pea amplitudes a_0=2.3~3.8 have been set in the simulation, corresponding to the peak laser of 1.1×10^{19}-3.0×10^{19}Wcm^{-2}. When a_0=2.3, only one electron bunch was injected into a stable bubble to form a quasi-monoenergetic electrons beam. With the increase of a_0, the second electron injection starts to appear. Our simulation illustrates

comprehensively the injection and acceleration processes, as shown in **Fig. 3** for the electron density (**Figs. 3a-3d**), the longitudinal wakefields and trapped electrons in the longitudinal phase space (**Figs. 3e-3h**), and the longitudinal profiles of the laser field (**Figs. 3i-3l**). At the beginning (**Figs. 3a** and **3e**), a bubble structure surrounded by a high-density sheath of compressed electron fluid is formed immediately behind the laser pulse. A bunch of electrons is self-injected and accelerated to approximately 300 MeV with a narrow energy spread due to the beam-loading effects. At this stage, the bubble structure remains intact and stable, allowing the first bunch to obtain stable acceleration with small-amplitude betatron oscillations. As the laser pulse propagates further into the plasma (**Figs. 3b** and **3f**), the first bunch is now quasi-monoenergetic with a higher energy.

During the laser propagation, the laser pulse front begins to steepen due to the relativistic self-phase modulation and the high-density sheath at the front of the laser pulse[24], as shown in **Figs. 3 i-l**. This steepening in turn leads to notable increase in the plasma wave amplitude and wavelength, which results in stretching and broadening of the bubble structure as shown in **Figs. 3c** and **3g** at 11.7 ps. At this time, the second wave bucket in the wakefield begins merging with the first bubble to form one large bubble During this merging process, a second bunch containing more electrons is injected into the large bubble and accelerated to even higher energy than the first bunch, as shown in **Figs. 3d** and **3h**. At this time, the first quasi-monoenergetic bunch is in the decelerating phase and its maximum energy is reduced. Comparing the simulation **Figs. 3d** and **3a**, the elongation of plasma wavelength during the bubble evolution makes the dephasing length for the second-injected electron bunch much longer (>1cm), leading to the higher energy than the normal dephasing limit. In the experiment, we have our laser pulse guided for 1 cm, therefore 1.4 GeV maximum electron energy gain is reasonable. This corresponds to the acceleration gradient (1.4 GV/cm) achieved for electrons. Interestingly, the second bunch strongly oscillates up and down at the tail of the large bubble with a amplitude as large as about 4 μm, while the first electron bunch experienced a negligibly-small transverse oscillations (~ 0.4 μm). The betatron oscillations can be found in **Figs. 3c-3d** and are traced in **Fig. 4** as explained in the following.

To understand the injection mechanism for the second electron bunch and the occurrence of the betatron oscillation, we have examined the evolution of the laser spot size from the simulations. As shown in **Fig. 4,** the laser spot size is slowly self-focused to a minimum value and then defocused and so on at the beginning. This kind of oscillation of the laser spot size is typical when the initial matching condition between the laser spot size and the laser amplitude $k_pR \sim k_pw = 2a_0^{1/2}$ is not satisfied[22], where k_p is the plasma wave number, R is the bubble radius and w is the laser spot size. However, a distinct feature appears later at t=8 ps when the oscillation period of the laser spot size reduces dramatically from 5 ps to 0.8 ps. Approximately at this time, the second bunch is injected and started to be accelerated. We call this new injection mechanism as the *oscillating bubble injection* (OBI) because the laser spot size oscillation causes the transverse oscillation of the bubble. During the OBI, the bubble oscillation can effectively couple to the transverse motion of the second electron bunch, starting a betatron resonance. As a result, the betatron transverse oscillation period coincides with the laser spot oscillation period. The OBI electrons are injected continuously, resulting in a broad energy spread. Meanwhile, the strong betatron oscillations of the OBI electron bunch lead to the generation of high-flux betatron radiation. These simulation results agree well with the experimental results for both the electron energy spectrum and the betatron X-ray emission.

It is experimentally demonstrated that the second injected electron bunch results in intense betatron X-ray emission. **Fig. 5** shows the X-ray photon flux measured in the experiment and calculated for small (0.4 μm) and large-amplitude (4 μm) betatron oscillations related to the first and second electron bunches correspondingly. Measured and calculated (for 4 μm amplitude) photon flux are shown to increase monotonically following the evolution of the second electron bunch. The calculated flux (green dashed line) for 0.4 μm amplitudes is far lower than what we observed experimentally. The results shown in **Fig. 5** clearly shows that intense and highly collimated X-ray emission can be ascribed mainly to the second-injected due to its high-energy and large transverse oscillation amplitude.

In conclusion, we have reported experimental observation of simultaneous generation of a quasi-monoenergetic electron bunch and a bright betatron X-ray emission, where the betatron X-rays are associated with another electron bunch with a broad energy spread and a large wiggling amplitude. Numerical simulation suggests that the quasi-monoenergetic electron bunch is injected and accelerated before the significant evolution of the laser pulse. However, the second electron bunch with a large energy spread is caused by oscillating bubble injection (OBI), which is resonant with the fast oscillation of the laser spot size. The large betatron oscillation amplitudes help to generate betatron X-ray radiation with peak brightness even larger than the third-generation synchrotron radiation sources. Our results suggest a way towards the concurrence of high-quality monoenergetic electron beams and bright betatron X-rays in a single shot laser wakefield accelerator. This is potentially interesting for “single-shot” ultrafast X-ray/electron pump-probe applications, such as phase contrast imaging, X-ray absorption fine structure and X-ray diffractions for warm dense matters with femtosecond time resolution.

METHODS

Laser system

The experiments were performed at the Jupiter Laser Facility, Lawrence Livermore National Laboratory, using the Callisto laser system. This Ti:sapphire system can delivers up to 200 TW in power in a 60 fs laser pulse at the central wavelength λ_0 of 806 nm. The laser pulse was focused with an *f*/12 off-axis parabolic mirror (OAP) to a vacuum spot of 18 μm (FWHM) in diameter with 35% energy contained at the full-width-half-maximum (FWHM). During the experiments, the peak laser power ranged from 60-155 TW on the target. In the focused region, the laser intensity was I=1.1×10^{19}-3.0×10^{19} Wcm^{-2}, which corresponded to the normalised vector potential a_0=2.3~3.8, where $a_0 = 8.6\times10^{-10}\lambda[\mu\mathrm{m}]I^{1/2}[\mathrm{W/cm^2}]$.

Gas jet

A supersonic helium gas jet nozzle was used, which is commercially available[26]. It has a rectangular shape of 10 mm in length and 1.2 mm in width, capable of produces a supersonic gas flow with a Mach number ~ 5. The gas densities generated from the gas jet was characterised using fluid dynamic calculations from the manufacturer[27]. The gas jet can generate well-defined uniform gas density profiles in the range of 1×10^{18} ~ 3×10^{19} cm^{-3} by changing the helium stagnation pressure. The laser was focused in vacuum at the front edge of the nozzle and at the height of 2 mm above the nozzle.

Diagnostics of electron beams and X-ray radiation

A 16-cm-long 0.98 Tesla dipole magnet, which was centred 112 cm from the exit of the gas jet, was set to disperse the electron beams. Four image plates (Fuji BAS-SR) were arranged as shown in **Fig. 1**. Image Plate 1 was placed to get the profile information of the electrons without the magnet. Image Plate 2 was pasted on the side of the magnet to measure the electron energy spectrum from 6 MeV to 100 MeV. Image Plates 3 and 4 were located at 155 and 205 cm away from the exit of the gas jet, respectively, which provided unambiguous energy spectrum measurement of the high-energy electrons[4,21]. A

1.5-mm-thick Be-window was used to seal the vacuum. This setup provided a total error in energy of 2.5% at 500 MeV. The published calibration of the Image Plate's photo-stimulated luminescence (PSL) provided information on the electron beam charge and the betatron photon flux[29,30]. Various filters (1.5-mm-thick Be-window, 30 μm Al-foils, 350-μm-thick Image plate, and 55 cm air) between the gas jet and Image Plate 3 allowed the detection of X-ray photons of > 7 keV in energy. To obtain critical energy of the X-rays, we use the method to calculate the transmission of x-rays through the different metal filters with a least squares[19]. To monitor the interaction volume, a charge coupled device (CCD) with a low-pass filter was used to observe high-harmonic emission of the target. This device measured the Thomson scattering to determine the interaction position and the time-integrated plasma channel length.

Particle-in-cell simulation

2D PIC simulations were performed using parameters that matched the experimental values with the code OOPIC, where a p-polarised laser pulse with duration of τ_{FWHM}=60 fs was focused into a pure gas target with a focal spot size of w_0 = 18 μm. A laser pulse with a normalised peak electric field of a_0=2.3~3.8 was launched at the entrance of the plasma of uniform Helium density at 4×10^{18} cm^{-3}. The laser pulse was assumed to have a perfect transverse Gaussian-shaped envelope.

REFERENCES

1 Leemans, W. P. *et al.* GeV electron beams from a centimetre-scale accelerator. *Nature Phys.* **2**, 696-699, (2006).

2 Wang, X. *et al.* Quasi-monoenergetic laser-plasma accelerationof electrons to 2 GeV. *Nat Commun* **4**,1988 (2013).

3 Cipiccia, S. *et al.* Gamma-rays from harmonically resonant betatron oscillations in a plasma wake. *Nature Phys.* **7**, 867-871, (2011).

4 Vainshtein, B. K. Diffraction Investigation of the Atomic-Structure of Matter. *Acta. Crystallogr. B* **47**, 145-154, (1991).

5 Tajima, T. & Dawson, J. M. Laser Electron-Accelerator. *Phys. Rev. Lett.* **43**, 267-270, (1979).

6 Mangles, S. P. D. *et al.* Monoenergetic beams of relativistic electrons from intense laser-plasma interactions. *Nature* **431**, 535-538, (2004).

7 Geddes, C. G. R. *et al.* High-quality electron beams from a laser wakefield accelerator using plasma-channel guiding. *Nature* **431**, 538-541, (2004).

8 Faure, J. *et al.* A laser-plasma accelerator producing monoenergetic electron beams. *Nature* **431**, 541-544, (2004).

9 Hafz, N. A. M. *et al.* Stable generation of GeV-class electron beams from self-guided laser-plasma channels. *Nature Photon.* **2**, 571-577, (2008).

10 Clayton, C. E. *et al.* Self-Guided Laser Wakefield Acceleration beyond 1 GeV Using Ionization-Induced Injection. *Phys. Rev. Lett.* **105**, 105003, (2010).

11 Esarey, E. *et al.* Synchrotron radiation from electron beams in plasma-focusing channels. *Phys.Rev. E* **65**, 056505 (2002).

12 Schoenlein, R. W. *et al.* Femtosecond X-ray pulses at 0.4 angstrom generated by 90 degrees Thomson scattering: A tool for probing the structural dynamics of materials. *Science* **274**, 236-238, (1996).

13 Spielmann, C. *et al.* Generation of coherent X-rays in the water window using 5-femtosecond laser pulses. *Science* **278**, 661-664, (1997).

14 Chen, L. M. *et al.* Study of x-ray emission enhancement via a high-contrast femtosecond laser interacting with a solid foil. *Phys.Rev. Lett.* **100**, 045004 (2008).

15 Chen, L. M. *et al.* Intense High-Contrast Femtosecond K-Shell X-Ray Source from Laser-Driven Ar Clusters. *Phys. Rev. Lett.***104**, 215004 (2010).

16 Schlenvoigt, H. P. *et al.* A compact synchrotron radiation source driven by a laser-plasma wakefield accelerator. *Nature Phys.* **4**, 130-133, (2008).

17 Fuchs, M. *et al.* Laser-driven soft-X-ray undulator source. *Nature Phys.* **5**, 826-829, (2009).

18 Kneip, S. *et al.* Bright spatially coherent synchrotron X-rays from a table-top source. *Nature Phys.* **6**, 980-983, (2010).

19 Rousse, A. *et al.* Production of a keV x-ray beam from synchrotron radiation in relativistic laser-plasma interaction. *Phys. Rev. Lett.* **93**, 135005(2004).

20 Mangles, S. P. D. *et al.* Controlling the spectrum of x-rays generated in a laser-plasma accelerator by tailoring the laser wavefront. *Appl. Phys. Lett.* **95**, 181106 (2009).

21 Chen, L. M. *et al.* Bright betatron X-ray radiation from a laser-driven-clustering gas target. *Sci. Rep.* **3**, 1912 (2013).

22 Lu, W. *et al.* Generating multi-GeV electron bunches using single stage laser wakefield acceleration in a 3D nonlinear regime. *Phys. Rev. Spec. Top.-Ac.* **10**, 061301 (2007).

23 Kneip, S. *et al.* Near-GeV Acceleration of Electrons by a Nonlinear Plasma Wave Driven by a Self-Guided Laser Pulse. *Phys. Rev. Lett.* **103**, 049901 (2009).

24 Faure, J. *et al.* Observation of laser-pulse shortening in nonlinear plasma waves. *Phys. Rev. Lett.* **95**, 205003 (2005).

25 Zhang, L. *et al.* Electron acceleration via high contrast laser interacting with submicron clusters. *Appl. Phys. Lett.* **100**, 014104(2012).

26 Semushin, S. & Malka, V. High density gas jet nozzle design for laser target production. *Rev. Sci.Instrum.* **72**, 2961-2965, (2001).

27 T. Hosokai, K. K., T. Watanabe, K. Yoshii, T. Ueda, A. Zhidokov, M. Uesaka,. Supersonic gas jet target for generation of relativstic electrons with 12 TW-50 fs laser pulse. *Proc. EPAC* 981-983, (2002).

28 Pollock, B. B. *et al.* Demonstration of a Narrow Energy Spread, similar to 0.5 GeV Electron Beam from a Two-Stage Laser Wakefield Accelerator. *Phys. Rev. Lett.***107**, 045001 (2011).

29 Nakanii, N. *et al.* Absolute calibration of imaging plate for GeV electrons. *Rev. Sci. Instrum.* **79**, 066102 (2008).

30 Mao, J. Y. *et al.* Application of a transmission crystal x-ray spectrometer to moderate-intensity laser driven sources. *Rev. Sci. Instrum.* **83**, 043104 (2012).

Acknowledgements

We would like to thank R. Cauble, S. Maricle, J. Bonlie and other Jupiter Laser Facility staffs at LLNL for laser and technical support and Joseph Nilsen for facilitating the experiment. This work was supported by the National Basic Research Program of China (Grant No. 2013CBA01501 and 2013CBA01504) and the NSFC (Grant No. 60878014, 10974249, 10925421, 11105217, 11121504 and 11175192). Part of this work was performed under the auspices of the U.S. Department of Energy by LLNL under Contract No. DE-AC52-07NA27344.

Author Contributions

L. M. C. and N. H. proposed the study. W. C. Y., L. Z., D. Z. L., L. M. C., N. H., J. D., L. N. S. conceived and realized the experiment. L. M. C. W. C. Y. and D. Z. L. analyzed the data. Y. M., L. M. C., D. Z. L. and K. H. performed the simulation. W. C. Y., L. M. C., Z. M. S. and N. H. wrote the paper. Z. M. S. and M. C. joined the discussion. J. Z supported the project.

Figure Captions

Figure 1: (colour) **Schematic of the experimental setup.** All of the Image Plates were wrapped with 25 μm Al foil. A 1.5-mm-thick Beryllium vacuum window was set 100 cm away from the gas jet to seal the vacuum. The lower-right inset shows the Thomson scattering image of the plasma channel.

Figure 2: (colour) **Accelerated electron beams, betatron X-rays and plasma channel measurement.** (***a-e***) show the spectrum characteristics of the electron beams and the betatron x-ray beam profile on Image Plate 3. (***f-j***) show the corresponding Thomson scattering obtained from the Top view CCD for the nozzle (***f-j***). The normalised vector potentials a_0 used in this work were 2.6 for (***a)*** and (***f)***, 2.8 for (***b)*** and (***g)***, 3.1 for (***c)*** and (***h)***, 3.3 for (***d)*** and (***i)***, and 3.6 for (***e)*** and (***j)***. (***k)*** is the deconvoluted spectra of electron energy for different channel lengths, where the inset **1** is the cut-off (maximum) energy of the electrons accelerated beyond 1GeV. The inset **2** in (***k)*** is a typical X-ray beam image with different filters, where the different filters are **I**, 78 μm Al; **II**, 250 μm Al; **III**, 129 μm Ti; **IV**, 264 μm Ti; **V**, 130 μm Cu; **VI**, 56 μm W.

Figure 3: (colour) **Typical snapshots of 2D PIC simulation results.** Frames (***a, e, i***) correspond to the time t=3.34 ps, frames (***b, f, j***) to t=8.13 ps, frames (***c, g, k***) to t=11.71 ps, and frames (***d, h, l***) to t=13.70 ps; (***a-d***) is the density distributions of the plasma electrons, and (***e-h***) is the kinetic energy of the electrons (black dots) and the longitudinal electric fields (blue lines). The longitudinal profiles of the laser electric fields are shown in (***i-l***). The incident laser peak amplitude is kept at a_0=3.6.

Figure 4: (colour) **The time evolution of the laser beam size and the transverse electron oscillations.** Initially the laser spot oscillates slowly until around t=8ps when the oscillation period drops dramatically. The injection due to the oscillating bubble (for the second electron bunch) starts afterwards, which is be accompanied by the resonantly-enhanced transverse oscillations of the electron bunch (blue curve).

Figure 5: (colour) **Scaling of electron energy and betatron X-ray photon number versus the channel length.** Red solid curve is the tendency of the central energy of the first injected electron bunch, while the black solid curve represents the cut-off (max.) energy of the second

injected bunch; The blue triangle is the X-ray photon number generated in the experiment; The yellow curve and the green curve give the photon numbers calculated by assuming a small amplitude and large amplitude electron transverse oscillations, respectively.

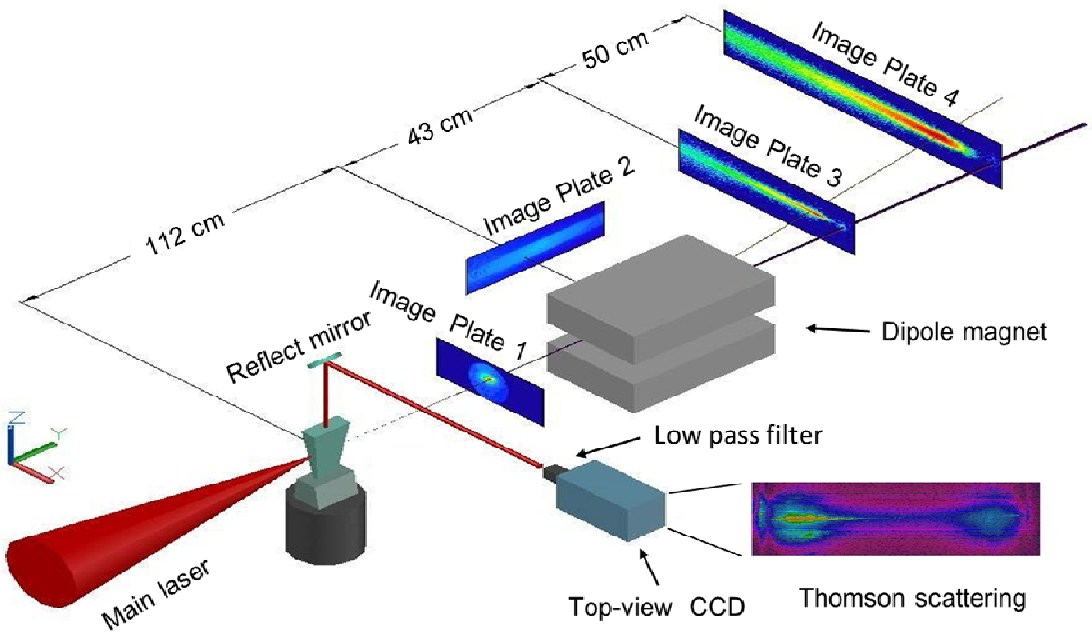
112 cm
43 cm
50 cm
Image Plate 4
Image Plate 3
Image Plate 2
Image Plate 1
Reflect mirror
Dipole magnet
Low pass filter
Main laser
Top-view CCD
Thomson scattering

Fig. 1

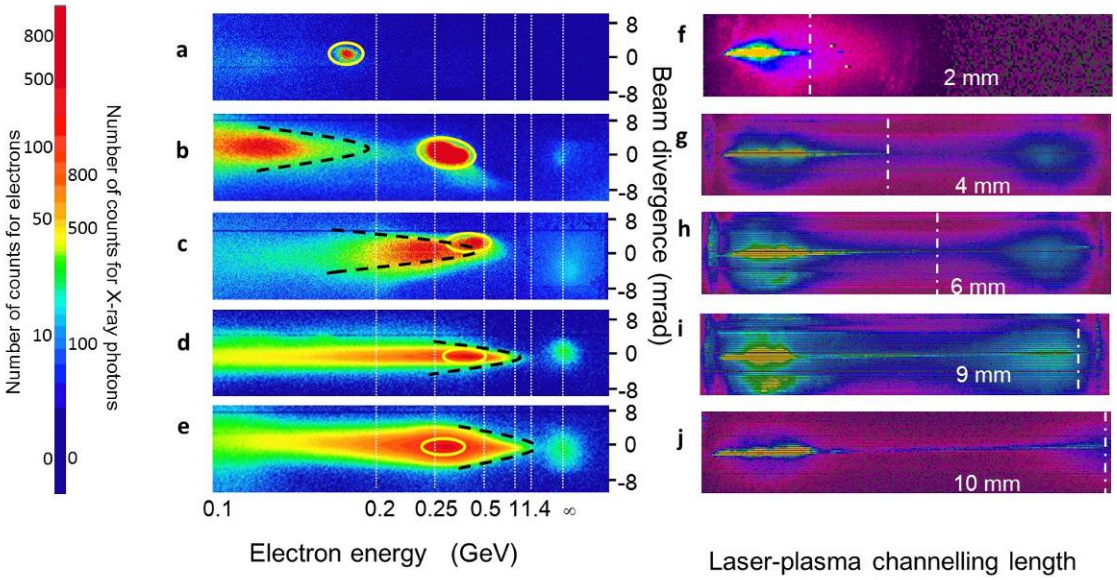

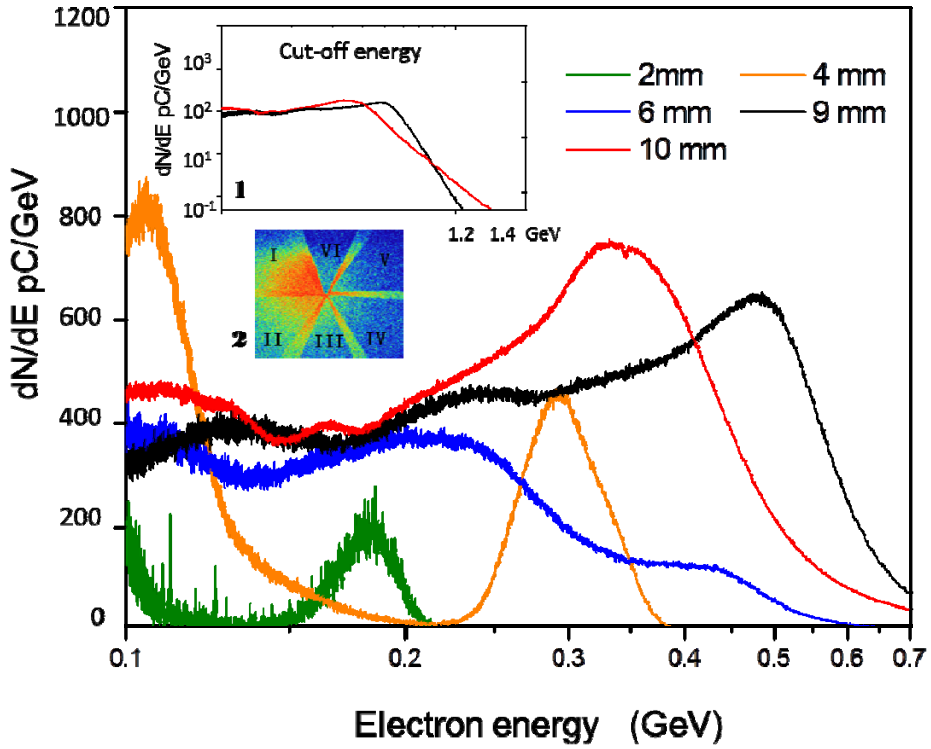

Fig. 2

【建议把 k 图中小图 2 放在 2mm，---10mm 的位置，使更醒目一点，标出 k】
【a，b，c，d，e 中黄色的圈起来的实线用白色虚线代替】

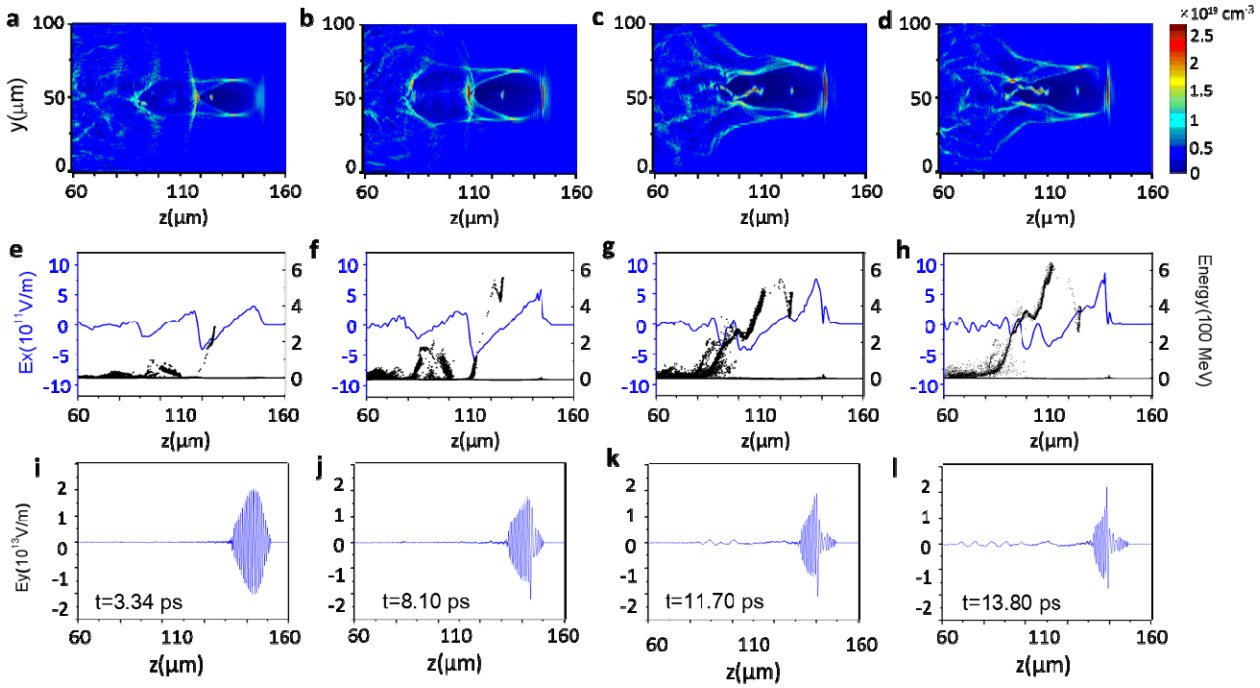
a
b
c
d
y(μm)
z(μm)
×10¹⁹ cm⁻³
2.5
2
1.5
1
0.5
0
e
f
g
h
Ex(10¹¹V/m)
Energy(100 MeV)
i
j
k
l
Ey(10¹³V/m)
t=3.34 ps
t=8.10 ps
t=11.70 ps
t=13.80 ps

Fig. 3

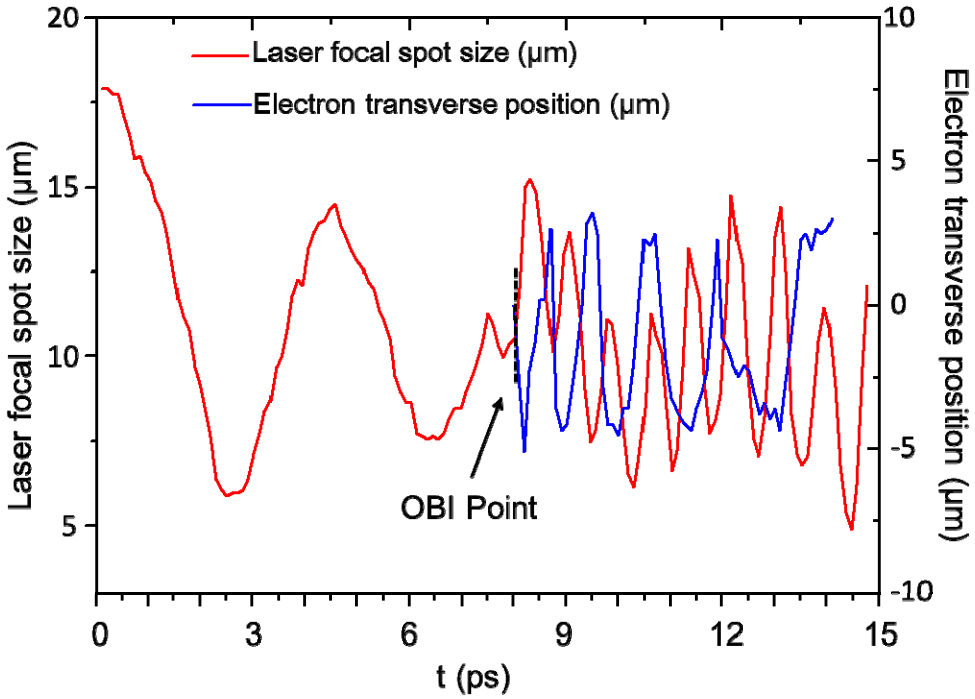
Laser focal spot size (μm)
Electron transverse position (μm)
OBI Point
Laser focal spot size (μm)
Electron transverse position (μm)
t (ps)
20
15
10
5
10
5
0
-5
-10
0
3
6
9
12
15

Fig. 4

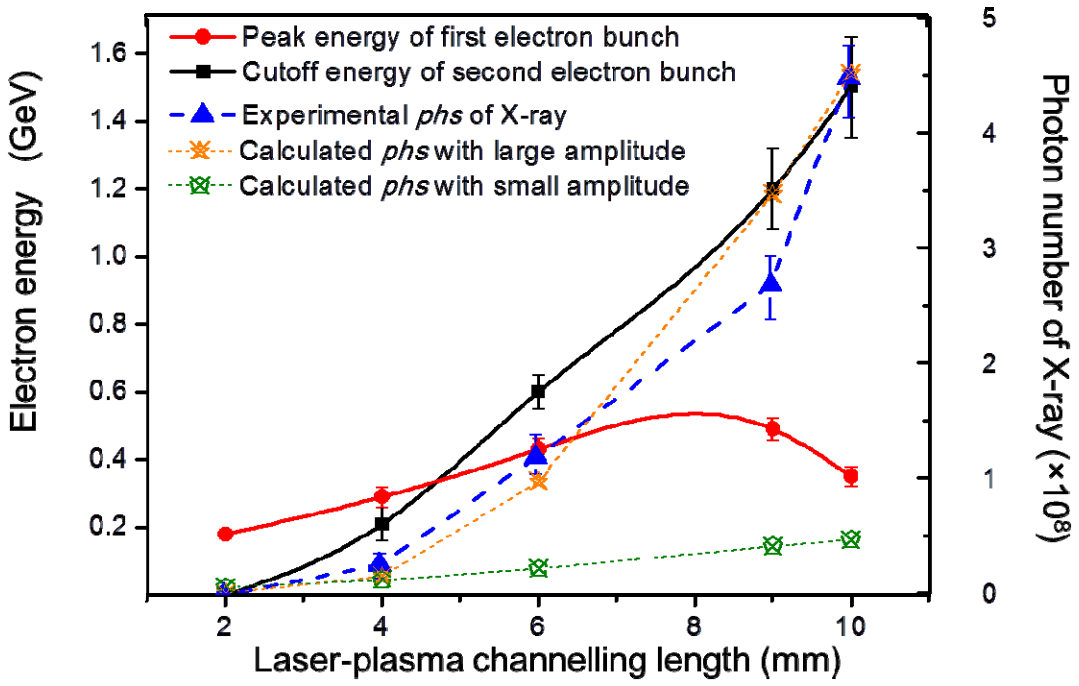

Fig. 5

【建议坐标轴上的数字大一点，图中的线条可以再粗一点】